

# How to get moving: lessons in eukaryotic motility from a prototypic model of cell polarization

Jasmine A. Nirody<sup>a</sup> and Padmini Rangamani,<sup>\*b</sup>

Mathematical models, with some simplifying assumptions, can provide clarity into the workings of complex biological systems. Despite their seeming simplicity, even so-called ‘minimal’ models can exhibit a diverse range of behavior in various regions of the parameter space. These models can be studied using simulations and analytical methods. Simulations are often parameter dependent and fall short of providing a complete understanding of the full range of system responses. Analytical approaches on the other hand provide a framework to study the entire phase space. Here, we outline a largely analytical method for studying reaction-diffusion models. Using a prototypic model of cell polarization, we characterize protein activation in response to an external stimulus and highlight the importance of phase-space analysis. We demonstrate how comprehensive treatment of the phase space can guide experimental design and supplement simulation studies. In order to make such analyses more accessible, we provide an easy-to-use graphical user interface to test the stability behavior of biological systems (available at <http://www.ocf.berkeley.edu/~jnirody>)<sup>†</sup>.

## 1 Introduction

Motility, and in particular directional cell movement, is fundamental for cellular function and survival. Cell migration is directed by external cues that serve as either attractants or repellants. Exposure to these cues sets into motion a series of intracellular responses, including the rearrangement of the actin cytoskeleton. This process ultimately culminates in an extension from the ‘leading’ edge of the cell. The formation of new *focal adhesions* at this protrusion lead to the contraction of the cell body and the detachment of the adhesive sites in the cell’s ‘rear’<sup>3,4,15,32</sup>. In order to lead to any coordinated movement, this process must be enacted by a polar cell—that is, a cell with a clearly designated ‘front’ and ‘back’.

The process of *cell polarization* is usually initiated first by the redistribution of signaling proteins, and then of the cytoskeletal elements within the cytoplasm<sup>3,4</sup>. A large variety of signaling proteins have been implicated in cell polarization and motility; these include Rho GTPases, MAP kinases, P13K, PTEN, and PAR proteins<sup>5,10,22,23,32</sup>. In this review, we focus on the involvement of the Rho family of GTPases, which are widely accepted as one of the key contributors to cell motility and the onset of polarity<sup>21</sup>.

Nearly 50 different members of the Rho family have been identified across the range of eukaryotes<sup>25</sup>. Rho GTPases exist in inactive, GDP-bound and active, GTP-bound states. The activation of these molecules serves as a molecular switch for

downstream processes, usually resulting in the polarization of cytoskeletal elements. Several experimental studies illustrate the dependence of cytoskeleton-mediated cell locomotion on members of this family: Rho has been shown to regulate the assembly of contractile actin-myosin filaments, and Rac and Cdc42 regulate actin polymerization to form protrusions for amoeboidal movement, as well as in the formation of lamellipodium and filopodium<sup>18</sup>. For more information on the role of this family of proteins in regulating downstream processes, we refer the interested reader to the comprehensive review by Raftopolou and Hall<sup>21</sup>.

Given their importance, it is unsurprising that the dynamics of these proteins has been of great interest, and have been studied both theoretically and experimentally<sup>1,6,7,27</sup>. Analysis of more extensive biochemical models of polarization than examined here can be found in several places in the literature<sup>2,22,32</sup>. Indeed, the Rho GTPase switch does not exist in isolation, and its interactions with downstream elements (including F-actin<sup>9,12</sup>) have been studied extensively. In the following, however, we focus on a comprehensive analysis the elegant and minimal model proposed by Mori *et al.*<sup>16</sup>.

This model exhibits a polarity-generating mechanism distinct from that of classical diffusion-driven (Turing) instabilities<sup>29</sup>, termed by the authors as ‘wave-pinning’. Polarization models relying primarily on Turing-type mechanisms are also plentiful in the literature<sup>13,19,27</sup>.

This model consists of the bidirectional conversion between active (A) and inactive (U) forms of a single protein. Through simulations, Mori *et al.* showed that their model exhibits many of the characteristic hallmarks of cell polarization<sup>16</sup>. First, when an initially unpolarized cell is given a directional stimulus, it responds by dividing its length into ‘front’ and ‘rear’ regions, defined by high and low concentration of active molecule, respectively. Second, a polarized cell is able

<sup>†</sup> Interactive Mathematica notebook for stability analysis of RD equations at <http://www.ocf.berkeley.edu/~jnirody>.

<sup>a</sup> Biophysics Graduate Group, University of California, Berkeley, Berkeley, CA 94720

<sup>b</sup> Department of Mechanical and Aerospace Engineering, University of California, San Diego, San Diego, CA 92093. Email: [padmini.rangamani@eng.ucsd.edu](mailto:padmini.rangamani@eng.ucsd.edu)

to reverse its polarity if subjected to a sufficiently strong opposing stimulus. Finally, polarity is maintained as an equilibrium state after removal of the transient stimulus. In a series of follow-up studies, the authors analyzed several further aspects of their model, including a comparison with models that display a primarily Turing-type mechanism of polarization<sup>10</sup>, extension of the model to consider downstream interactions with actin<sup>12</sup>, and the effects of stochasticity on the wave-pinning mechanism<sup>30</sup>.

In the following, we outline a largely *analytic* treatment of this model, which is made possible by the simplicity of its formulation. Despite this simplicity, however, the model displays rich dynamics. Using techniques from dynamical systems and bifurcation theory, we explore the parameter space and divide it into regions based on the characteristics of model equilibria within them. The ability to fully explore and properly characterize these regimes is a benefit of this analysis in comparison to simulation-based studies. We note that the analysis presented in this paper is largely generalizable, and can be applied to various biochemical models. To this end, we provide a user-friendly graphical user interface (GUI) to test the stability behavior of other biological systems of interest (available at <http://www.ocf.berkeley.edu/~jnirody>)<sup>†</sup>.

In particular, we use our analysis to review and explain the following aspects of cell polarization:

1. How does localization of the active form to the membrane (modeled in the WPP model as a 100-fold difference in diffusion rates between U and A) facilitate cell polarization?
2. How does the size of a cell affect its ability to polarize?
3. Is spontaneous polarization observed in the absence of an external directional stimulus?
4. Can polarization occur through more than one intrinsic mechanism?

## 2 Model overview

Biological systems are often overwhelmingly complex, but the emergence of conserved, key motifs can point to a set of ‘minimal’ properties required for a dynamic behavior. One such motif has been the central role of Rho GTPases in regulating cell polarization and motility. Prototypic models which capture the fundamental properties of the system they intend to emulate are powerful for studying such complex systems. In particular, their simplicity makes them mathematically tractable and amenable to comprehensive analysis. In the following, we give an overview of a particularly simple and elegant model of cell polarization, which we term the ‘wave-pinning polarization’ (WPP) model.

The WPP model was first proposed in 2008 by Mori *et al.* as fulfilling a ‘minimal’ set of requirements for cell polarization and the onset of motility<sup>11,16</sup>. Figure 1A shows an overview of the model: an inactive form of a protein (U) is converted to the active form (A) with some rate  $k_{\text{on}}$ , with the reverse reaction occurring with some rate  $k_{\text{off}}$ . Additionally, the active form provides positive feedback, facilitating its own formation. The nonlinearity provided by this feedback is necessary for many of the important properties of the model.

As shown in Figure 1A, the base reactions are modeled around the bidirectional conversion between two forms of a single protein. For ease of notation, we call the concentrations of the active and inactive forms  $a$  and  $u$ . The kinetics of this system are

$$\begin{aligned} \frac{da}{dt} &= f(a, u) \\ &= \underbrace{k_{\text{on}}u}_{\text{activation}} - \underbrace{k_{\text{off}}a}_{\text{inactivation}}, \end{aligned} \quad (1)$$

The choice of function  $f(a, u)$  is relatively arbitrary, as long as it fulfills the criteria described previously; namely, that there exists cooperative feedback from A onto its own production. We choose the rate of activation  $k_{\text{on}}$  to be a basal rate  $k_0$  (units of 1/time,  $\text{s}^{-1}$ ) combined with a Hill function with saturation parameter  $K$  (units of concentration, mM) and dimensionless maximal rate  $\gamma$ :

$$k_{\text{on}} = \underbrace{k_0}_{\text{basal activation rate}} + \underbrace{\frac{\gamma a^2}{K^2 + a^2}}_{\text{cooperative feedback}}. \quad (2)$$

The Hill coefficient  $n_H = 2$  is chosen to ensure the existence of a bistable parameter range. Then:

$$f(a, u) = u \underbrace{\left( k_0 + \frac{\gamma a^2}{K^2 + a^2} \right)}_{\text{activation}} - \underbrace{k_{\text{off}}a}_{\text{inactivation}}. \quad (3)$$

Assuming there is no flux in or out of the system, mass conservation requires that:

$$\begin{aligned} \frac{du}{dt} &= -\frac{da}{dt} \\ &= -f(a, u). \end{aligned} \quad (4)$$

To find *steady state* solutions  $(a^*, u^*)$  of this system, we must solve for  $f(a, u) = 0$ . Additionally, to enforce mass conservation, we impose the constraint  $p = u_0 + a_0 = u(t) + a(t)$ , where  $p$  is a constant denoting the total amount of protein. This means that an equilibrium point  $(a^*, u^*) = (a^*, p - a^*)$  must satisfy

$$(p - a^*) \left( \frac{\gamma a^{*2}}{K^2 + a^{*2}} \right) = k_{\text{off}} a^*. \quad (5)$$

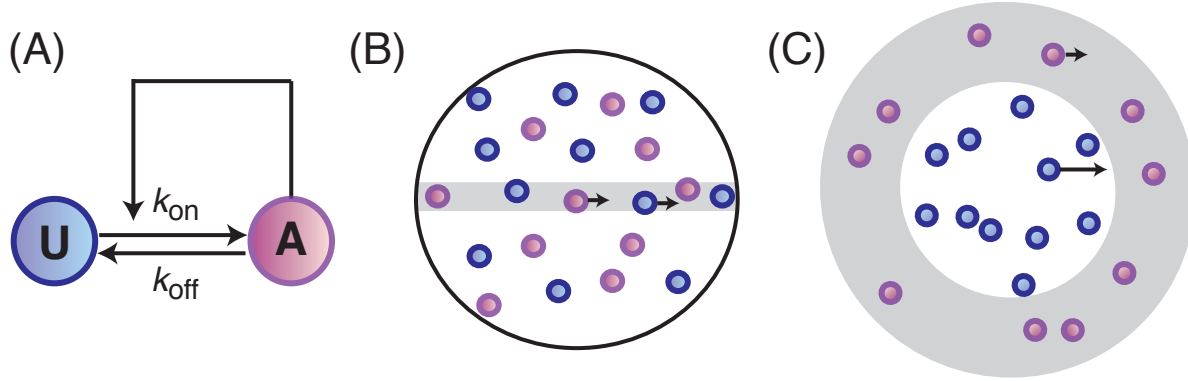


**Fig. 1** Schematic of the WPP model. (A) Purely nonspatial model corresponds to a well-mixed system. The model consists of an interconversion between inactive (U) and active (A) forms of a single protein. The active form effects a positive feedback on its own production; in the WPP model, this feedback takes the form of a cooperative Hill function. An extended one-dimensional spatial model can be representative of (B) two cytoplasmic species or (C) one cytoplasmic and one membrane-bound species, depending on the relative diffusion coefficients of the forms.

The solutions to the above equation can be visualized as intersections between a sigmoidal curve (the left hand side) and a straight line (the right hand side). There are at most three such intersections. In the following, we generally restrict ourselves to a parameter space where these three solutions exist and are real-valued; we label them in increasing order as  $a_1^* < a_2^* < a_3^*$ .

The above model only considers only *homogenous* solutions, which exhibit no spatial structure. However, spatial heterogeneity is nearly ubiquitous in real biological systems. Luckily, it is relatively straightforward to remove the assumption of a well-mixed system by considering a *reaction-diffusion system* with the kinetics of the well-mixed WPP model.

We consider a one-dimensional segment ( $0 \leq x \leq L$ ), which can serve as an approximation of a transection of the cell. Depending on the relative values of the diffusion coefficient, this extension can serve to model two cytoplasmic species (Figure 1B) or one cytoplasmic and one membrane-bound species (Figure 1C). As before,  $u$  and  $a$  are the concentrations of U and A, both in units of molecules/length:

$$\frac{da}{dt} = D_a \frac{\partial^2 a}{\partial x^2} + f(a, u) \quad (6)$$

$$\frac{du}{dt} = D_u \frac{\partial^2 u}{\partial x^2} - f(a, u). \quad (7)$$

Reaction-diffusion models are ubiquitous in biology, particularly in systems which give rise to spatial patterning<sup>13</sup>. Indeed, many such models have been suggested for the generation of cell polarity<sup>13,19,27</sup>. Despite their seeming simplicity, the difficulty in analyzing (and comparing) these *partial differential equation* (PDE) models comes from the richness of their behavior as parameters are varied, especially when compared to the phase-space of their reaction-only *ordinary differential*

*equation* (ODE) counterparts. This daunting complexity often leads to these models being studied primarily through simulations, which provide instant but ultimately transient gratification: while we gain insight into the behavior of these systems, the variety of their behaviors across parameter space nearly assures that we cannot grasp their full capabilities through simulation alone. In the following section, we outline an *analytic* protocol for the study of reaction-diffusion systems, particularly those corresponding to cell polarization. Using the WPP model as an example, we divide the parameter space into regions and characterize the typical behavior of the system within them. We emphasize that the steps discussed in this article are highly generalizable, and we hope to highlight how such comprehensive treatments of mathematical models in biology are powerful and insightful.

### 3 Phase-space analysis

After their initial proposal of the WPP model<sup>16</sup>, the authors considered several important extensions<sup>10,17,30</sup>. However, a full characterization of the equilibrium behavior of the system as a function of the basal rate of activation  $k_0$  and the average amount of total protein  $p$  has not yet been adequately discussed. In this section, we outline such a characterization. The mathematical basis of such analyses can be found in the fundamental book by Strogatz<sup>26</sup>. Computations were done in Mathematica and MATLAB; all associated scripts will be made available as a user-friendly GUI at [www.ocf.berkeley.edu/~jnirody](http://www.ocf.berkeley.edu/~jnirody)<sup>†</sup>.

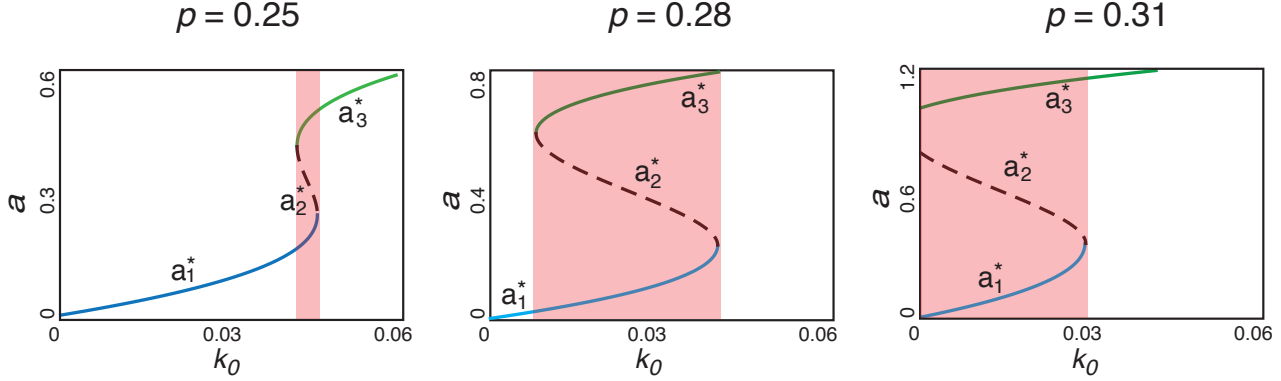


**Fig. 2** Equilibrium curves for each of the three steady states in the WPP model. For all of the following plots, we choose:  $\gamma = 1$ ,  $k_{\text{off}} = 1$ ,  $K = 1$  and vary the average amount of total protein  $p$ . The two stable steady states  $a_1^*$  and  $a_3^*$  are shown as solid blue and green lines, respectively; the unstable steady state  $a_2^*$  is shown as a dashed line. For a range of  $k_0$ , all three steady states exist and are real-valued; this region is shaded in red; this range increases with  $p$ , eventually resulting in an *irreversible* system response when it reaches  $k_0 = 0$ .

### 3.1 Well-mixed model

We first begin with the (relatively) easier task of analyzing the reaction-only ODE model before considering the full reaction-diffusion system. Recall that the WPP model has three steady states, which we denote  $(a_1^*, u_1^*)$ ,  $(a_2^*, u_2^*)$ , and  $(a_3^*, u_3^*)$ . To assess the stability of each of these steady states, we look at the *Jacobian matrix* of the system:

$$J = \begin{pmatrix} f(a, u)_a & f(a, u)_u \\ -f(a, u)_a & -f(a, u)_u \end{pmatrix} \\ = \begin{pmatrix} \frac{2auK^2\gamma}{(a^2+K^2)^2} - k_{\text{off}} & k_0 + \frac{\gamma a^2}{K^2+a^2} \\ -\frac{2auK^2\gamma}{(a^2+K^2)^2} + k_{\text{off}} & -k_0 - \frac{\gamma a^2}{K^2+a^2} \end{pmatrix}.$$

Here,  $f_a$  and  $f_u$  denote the partial derivatives of  $f(a, u)$  with respect to  $a$  and  $u$ , respectively. The linearization of the reaction terms around an equilibrium point  $(a^*, u^*)$  is simply  $J|_{(a^*, u^*)} [da \ du]^T$ , where  $J|_{(a^*, u^*)}$  represents the Jacobian matrix evaluated at  $(a^*, u^*)$ . An equilibrium point is said to be stable if the eigenvalues of the  $J|_{(a^*, u^*)}$  all have real parts less than or equal to zero and unstable if any one eigenvalue has a real part greater than zero.

Example equilibrium curves for  $\gamma = 1$ ,  $k_{\text{off}} = 1$ ,  $K = 1$  are shown for various values of average total protein  $p$  in Figure 2. For the WPP model,  $a_1^*$  and  $a_3^*$  are stable (shown as blue and green solid lines, respectively), while  $a_2^*$  is unstable (shown as a black dashed line).

For certain choices of parameters, both stable steady states exist; this is called the *bistable regime*. Within this region, either of the two steady states may be reached for the same set of kinetic parameters, depending on the initial conditions of the system (i.e., the ‘starting’ concentrations).

Bistability is a common feature in biochemical reaction networks, particularly those containing positive feedback loops<sup>31</sup>.

In this way, positive feedback loops may allow for a sustained cellular response to a transient external stimulus<sup>31</sup>, a central feature in cell polarization. To illustrate this, consider the basal rate parameter  $k_0$  as a function of an external stimulus  $S$  (i.e.,  $k_0 = k_0^* S$ ). Now, we can look to the plots in Figure 2 as dose-response curves — the cell responds to external stimulus  $S$  by producing the activated protein A.

As  $S$  (and consequently  $k_0$ ) is slowly increased, the concentration of A follows along the curve corresponding to  $a_1^*$  (blue) until it crosses the bistable region, after which the equilibrium value is the larger  $a_3^*$  (green). If the stimulus is removed, and the level of  $S$  decreases, the higher-valued equilibrium is maintained within the bistable region; this behavior, where the dose-response relationship is in the form of a loop rather than a curve, is called *hysteresis*. If the bistable regime is large enough, in particular if it extends to  $k = 0$ , an essentially irreversible response to transient stimuli may be elicited (as is seen for  $p = 0.31$  in Figure 2).

Figure 3 shows the bistability region for the WPP model as the total average protein concentration  $p$  and the basal activation rate  $k_0$  are varied. From the sloping shape of the bistable region, we can see that for sufficiently high values of total protein (for the set of parameters in Figure 3,  $p \geq 3$ ), an ‘irreversible’ response may be generated: both steady states are stable even when the stimulus is removed, at  $k_0 = 0$ . The simulation parameters chosen by Mori *et al.* are shown as a purple dot.

### 3.2 1-D spatial model

Having characterized the bistable regime of the well-mixed model, we now turn our attention to the full reaction-diffusion system. The homogenous equilibria also serve as steady states for the spatially extended system and as before, we are inter-

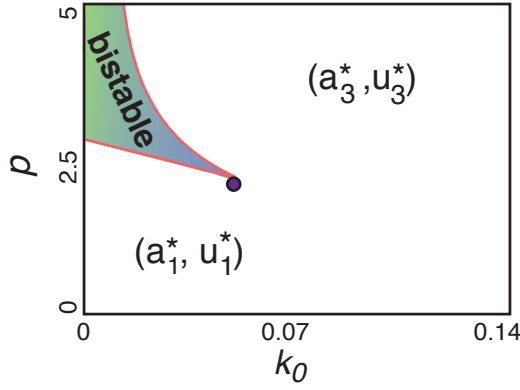


**Fig. 3** The extent of the bistable region in  $(k_0, p)$  space for the well-mixed model. In unshaded regions, only a single stable steady state (either  $(a_3^*, u_3^*)$  or  $(a_1^*, u_1^*)$ ) exists. Within the shaded region, both steady states exist and are stable. The system may tend to either state, dependent on initial conditions. The parameter set used in the simulations by Mori *et al.*<sup>16</sup> is shown as a purple point.

ested in their stability throughout the parameter space.

Recall that for the spatially homogenous system, we turned to the Jacobian to analyze the linear stability of these states under small perturbations from equilibrium. The linearized spatially-extended equation now has the form

$$\frac{\partial}{\partial t} \begin{bmatrix} \partial a \\ \partial u \end{bmatrix} = \begin{bmatrix} D_A & 0 \\ 0 & D_U \end{bmatrix} \frac{\partial^2}{\partial x^2} \begin{bmatrix} \partial a \\ \partial u \end{bmatrix} + J \begin{bmatrix} \partial a \\ \partial u \end{bmatrix}, \quad (8)$$

where  $J$  is the Jacobian for the reaction equations, as before. In order to analyze the stability of this system with respect to perturbations, we must first note that now these perturbations depend both on time and space. A convenient form for such perturbations is  $[\partial a \ \partial u] = [\partial a^* \ \partial u^*] e^{\lambda t} e^{ikx}$ , where the term  $e^{ikx}$  is a common way to represent a spatial wave, with  $k$  as the wavenumber. Substituting this into the linearized equation (8) leads to the Jacobian of the spatially extended system

$$J^* = \begin{pmatrix} f(a, u)_a - D_A k^2 & f(a, u)_u \\ -f(a, u)_a & -f(a, u)_u - D_U k^2 \end{pmatrix},$$

with eigenvalues

$$\sigma^\pm = \frac{1}{2} \left[ (f_a - f_u - (D_A + D_U)k^2) \pm \sqrt{(f_a - f_u - (D_A + D_U)k^2)^2 - 4(D_A D_U k^4 + (D_A f_u - D_u f_a)k^2)} \right] \quad (9)$$

As the expressions for the eigenvalues now contain the additional unknown  $k$ , we are now interested in a *family of solutions*, one for each wavenumber. The eigenvalues for the nonspatial system are achieved when  $k = 0$ , and are given by

$\sigma^- = f_a - f_u$  and  $\sigma^+ = 0$ ; therefore any spatially homogenous perturbation will relax back to the spatially uniform steady state. We are instead interested in the emergence of heterogeneous patterns that occur via perturbations within a finite range of critical wavenumbers  $0 \leq k_c \leq k_{\max}$ . The value of these crit-

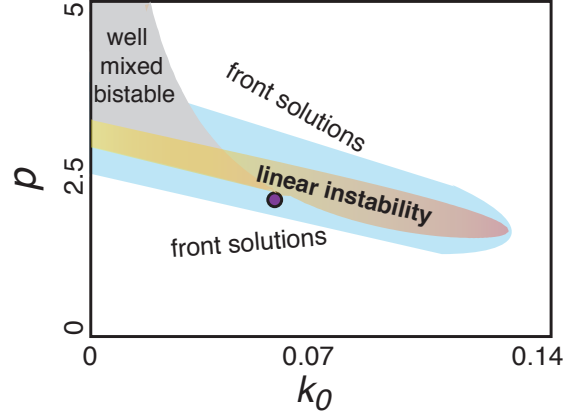


**Fig. 4** Parameter space topology for the full PDE model when  $D_U = 10 \mu\text{M}^2\text{s}^{-1}$  and  $D_A = 0.1 \mu\text{M}^2\text{s}^{-1}$ . The region of linear instability is shown shaded in orange for wavenumber  $k = 0.2$ . This corresponds to a perturbation of length  $L = \frac{2\pi}{k} \approx 30 \mu\text{M}$ . Smaller values of  $k$  result in an expansion of the linear instability region; larger values of  $k$  result in the region shrinking. An additional domain is shown shaded in blue, in which front-like solutions are supported when given a sufficiently strong (or spatially graded) perturbation. The parameter choice made by Mori *et al.* (purple point) lies in this region.

ical wavenumbers becomes important when we are faced with a finite domain size. Since cells are of finite size, we want to investigate how the length of the domain affects the system response. This is because the spatial pattern that emerges from an instability corresponding to a wavenumber  $k$  has wavelength  $\omega = \frac{2\pi}{k}$ ; accordingly, for finite systems, only values of  $k$  above a certain threshold will generate any meaningful spatial patterns.

The region of ‘linear instability’ is highlighted in orange in Figure 4 for  $k = 0.2$ . This corresponds to a pattern of wavelength  $\omega = \frac{2\pi}{k} \approx 30 \mu\text{M}$ . This length scale is intermediate among the motile eukaryotic cells that use Rho GTPases to generate polarity. In this region, one or both of the steady states,  $(a_1^*, u_1^*)$  and  $(a_3^*, u_3^*)$ , lose stability with respect to a non-homogenous perturbation as shown above (see Figure 5).

We note that the region computed is for diffusion coefficients  $D_U = 10 \mu\text{M}^2\text{s}^{-1}$  and  $D_A = 0.1 \mu\text{M}^2\text{s}^{-1}$ . A similar parameter topology (with slightly larger regions of instability) was found in a reduced one-species model where infinite cytoplasmic diffusion was assumed<sup>28</sup>. The disparity in diffusion coefficients assumed in Figure 4 presupposes the compartmentalization of

the two species: a protein diffuses far more slowly on the membrane than in the cytosol (here, we assume the ratio of diffusion coefficients to be  $\approx 0.01$ <sup>20</sup>). In the following sections, we will assess the importance of this presumption. In addition to the region of linear instability, the parameter space for the full model can admit a surrounding region where front-like solutions are observed. In this region, a stalled wave can appear when the system is subjected to a directed stimulus (e.g., a gradient) or if the domain exhibits some intrinsic polarity at  $t = 0$ . The parameters chosen by Mori *et al.* fall within this region; their simulations demonstrate that this ‘intrinsic polarity’ may arise via sufficiently noisy initial conditions<sup>16</sup>.

The boundaries to this regime are calculated by solving the Maxwell condition and finding the ranges of  $u$  that admit a stalled wave<sup>16</sup>:

$$I(b) = \int_{a_-}^{a_+} f(a, u) da = 0. \quad (10)$$

We then use the mass conservation condition to compute this region in  $(k_0, p)$  space. While this is not analytically feasible for the WPP model, numerically solving the integral provides an accurate characterization of this region.

The method outlined here is not specific to the WPP model, or even to models of cell polarity. To make such a phase-space analysis more accessible to the biological community, we provide an easy-to-use GUI to allow readers to analyze the stability properties of other systems of interest.

## 4 Key take-away points

The analysis above provides us significant insight into the behavior of the WPP model throughout the parameter space (Figure 4). Using this, we can point out several notable properties of the model as they pertain to cell polarization.

We note that the below properties are predicted using analyses performed on a 1D spatial model. Extension of the model to three, or even two, dimensions may (and likely do) result in different behaviors<sup>5</sup>. However, an analytic treatment of higher-dimensional spatial models is rarely possible, and thus the comprehensive analysis of a reduced model in one spatial dimension lays the foundation for simulation studies in higher dimensions.

1. **Importance of compartmentalization:** The Rho GTPase family is large and varied, and is present in eukaryotes spanning from *C. elegans* to humans. However, one common feature of these proteins is *compartmentalization*: the active form is bound to the membrane, while the inactive form diffuses in the cytoplasm<sup>21</sup>. This feature has been shown to be important for cell polarization<sup>10,16,17</sup>. We illustrate the necessity of membrane localization by considering how the phase space of the WPP model in Figure 4 changes if both species are contained in the cytoplasm.

Qualitatively, the dependence of polarization on compartmentalization is relatively intuitive. As A and U constitute GTP- and GDP-bound versions of a single protein, their cytoplasmic diffusion rates are likely very similar. Given this, one would not expect the formation of any sort of regular pattern with no initial spatial structure.

We show this quantitatively by defining the ratio of the diffusion rates  $R_D = D_A/D_U$ , and considering the effect of this quantity on the regimes allowing spatially heterogeneous solutions. For one membrane-bound and one cytoplasmic species, we take this ratio to be  $\approx 0.01$ <sup>20</sup>.

When  $R_D = 1$ , no spatially heterogeneous patterns can be generated, and this region disappears altogether. However, as  $R_D$  decreases, spatial patterns are supported for a finite range of wavenumbers (Figure 5)<sup>17</sup>. As the rate of diffusion of U increases, the maxima of  $\sigma(k)$  move towards  $k = 0$ , eventually displacing the uniform steady state in the limit  $D_U \rightarrow \infty$ <sup>28</sup>. This trend is not symmetric — as  $R_D$  increases from 1, there is no consequent extension of the multistable regime. This is similar to the formation of Turing patterns in local excitation, global inhibition models; for an overview of this brand of models with respect to cell polarization, we refer the reader to several excellent reviews<sup>5,10,16</sup>.

2. **Benefit of being big:** In addition to the importance of different diffusion rates between active and inactive forms, we can use the fact that the range of critical wave numbers is bounded above to consider the existence of a corresponding *lower bound* on the length of the cell  $L$ .

The value of the maximum critical wavenumber  $k_{\max}$  for a feasible value of  $R_D$  is quite low (Figure 5). This suggests that smaller cells are less sensitive to polarization, while larger cells are able to respond more robustly. Interestingly, this result has been observed experimentally: cells were found to become significantly more sensitized as they were flattened in a confined channel<sup>8,14</sup>.

3. **Spontaneous polarization:** Recall that  $k_0$  can be written as a function of the concentration of some stimulus  $S$ :  $k_0(S) = k_0^* S$ . This formulation allows us to characterize parameter values which allow for *spontaneous polarization* in the absence of a directed external stimulus.

Certain, but not all, cells are able to spontaneously self-polarize. In the WPP model, we can by considering the regimes crossed in Figure 4 by the line  $k_0 = 0$ . We see that polarization in the absence of a stimulus is possible if the value of  $p$  is sufficiently high. This is consistent with experimental observations that the constitutive expression of Rho GTPases result in extension of randomly oriented lamellipodia and membrane ruffling<sup>24</sup>.

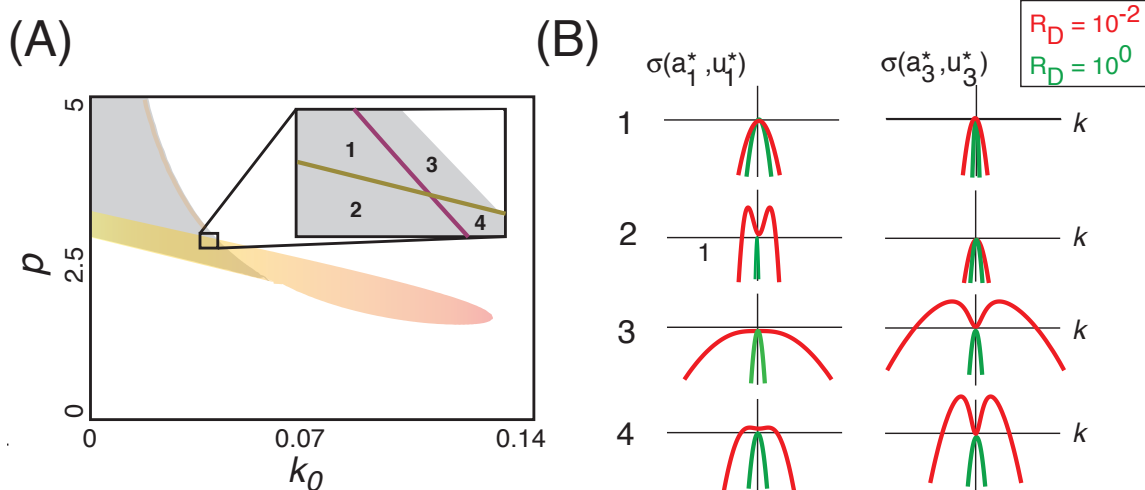


**Fig. 5** Examination of the rise of Turing patterns by loss of stability given critical wave numbers  $k$ . **(A)** A small segment of the parameter space is highlighted for the full spatial WPP model, showing regions where neither (region 1), one (regions 2 and 3), or both (region 4) of the equilibrium points become unstable. **(B)** An illustration of the loss of the linearly instability regime as  $R_D$  approaches 1. Plots show the magnitude of the real part of the rightmost eigenvalue for both equilibria within each of the regions highlighted in **A**. Plots are shown for  $k \in [-1, 1]$ . When  $R_D = 10^{-2}$ , corresponding to the localization of the active form to the membrane, a finite range of critical wavenumbers is observed; this range disappears when  $R_D = 1$ .

4. **Polarization strategies:** The parameter space topology for the WPP model contains two distinct regions that allow for non-homogenous equilibrium solutions. Because of the choice of parameters in Mori *et al.*<sup>16</sup>, the system behavior in only one of these regions, corresponding to stalled-wave solutions (shaded in blue in Figure 4) was explored. The fact that these solutions were not initially found by a purely simulation-based study further emphasizes the need for comprehensive analytic treatment of biological models.

In general, Turing patterns form more easily (i.e., in response to far smaller perturbations) than patterns formed by a wave-pinning mechanism. However, they occur on a far slower timescale<sup>5,10,16</sup>. The existence of a Turing-like instability regime in addition to a region which admits stalled-wave solutions presents cells with multiple strategies for polarization.

## 5 Conclusions

The WPP model captures many of the inherent properties observed in cell polarization, including response to a spatial gradient, sustained polarization after removal of a transient stimulus, and spontaneous polarization in the absence of any external cues. In the above, we give an overview of the full range of the system responses through a comprehensive phase-space analysis.

Prototypic ‘minimal’ models are commonly used to study biological phenomenon. For systems involving spatial patterning, such models are often of the reaction-diffusion type. As the behavior of these systems can vary widely with parameter choice, simulation studies are often unsatisfying in that they only provide a small peek into the full capabilities of these models. In the above, we outline the steps for a comprehensive analytic treatment of an example minimal model for cell polarization. Additionally, a user-friendly interface for implementing such a treatment for generic reaction-diffusion systems is provided online as a supplement. We show the usefulness of such a protocol, in that it illuminates several features of the model which are difficult to observe via simulation alone.

## References

- 1 A Bishop and Alan Hall. Rho gtpases and their effector proteins. *Biochem. j.*, 348:241–255, 2000.
- 2 Adriana T Dawesa and Leah Edelstein-Kesheta. Phosphoinositides and rho proteins spatially regulate actin polymerization to initiate and maintain directed movement in a 1d model of a motile cell. 2006.
- 3 Hans-Günther Döbereiner, Benjamin Dubin-Thaler, Grégory Giannone, Harry S Xenias, and Michael P Sheetz. Dynamic phase transitions in cell spreading. *Physical review letters*, 93(10):108105, 2004.
- 4 Hans-Günther Döbereiner, Benjamin J Dubin-Thaler, Gregory Giannone, and Michael P Sheetz. Force sensing and generation in cell phases: analyses of complex functions. *Journal of Applied Physiology*, 98(4):1542–1546, 2005.



- 5 Leah Edelstein-Keshet, William R Holmes, Mark Zajac, and Meghan Dutot. From simple to detailed models for cell polarization. *Philosophical Transactions of the Royal Society B: Biological Sciences*, 368(1629):20130003, 2013.
- 6 Ting Gong, Yuan Liao, Fei He, Yang Yang, Dan-Dan Yang, Xiang-Dong Chen, and Xiang-Dong Gao. Control of polarized growth by the rho family gtpase rho4 in budding yeast: Requirement of the n-terminal extension of rho4 and regulation by the rho gtpase-activating protein bem2. *Eukaryotic cell*, 12(2):368–377, 2013.
- 7 Alan Hall. Rho gtpases and the actin cytoskeleton. *Science*, 279(5350):509–514, 1998.
- 8 William R Holmes, Benjamin Lin, Andre Levchenko, and Leah Edelstein-Keshet. Modelling cell polarization driven by synthetic spatially graded rac activation. *PLoS computational biology*, 8(6):e1002366, 2012.
- 9 WR Holmes, AE Carlsson, and L Edelstein-Keshet. Regimes of wave type patterning driven by refractory actin feedback: transition from static polarization to dynamic wave behaviour. *Physical biology*, 9(4):046005, 2012.
- 10 Alexandra Jilkine and Leah Edelstein-Keshet. A comparison of mathematical models for polarization of single eukaryotic cells in response to guided cues. *PLoS computational biology*, 7(4):e1001121, 2011.
- 11 Athanasius FM Marée, Alexandra Jilkine, Adriana Dawes, Verónica A Grieneisen, and Leah Edelstein-Keshet. Polarization and movement of keratocytes: a multiscale modelling approach. *Bulletin of mathematical biology*, 68(5):1169–1211, 2006.
- 12 May Anne Mata, Meghan Dutot, Leah Edelstein-Keshet, and William R Holmes. A model for intracellular actin waves explored by nonlinear local perturbation analysis. *Journal of theoretical biology*, 334:149–161, 2013.
- 13 Hans Meinhardt. Orientation of chemotactic cells and growth cones: models and mechanisms. *Journal of Cell Science*, 112(17):2867–2874, 1999.
- 14 Jason Meyers, Jennifer Craig, and David J Odde. Potential for control of signaling pathways via cell size and shape. *Current biology*, 16(17):1685–1693, 2006.
- 15 TJ Mitchison and LP Cramer. Actin-based cell motility and cell locomotion. *Cell*, 84(3):371–379, 1996.
- 16 Yoichiro Mori, Alexandra Jilkine, and Leah Edelstein-Keshet. Wave-pinning and cell polarity from a bistable reaction-diffusion system. *Biophysical journal*, 94(9):3684–3697, 2008.
- 17 Yoichiro Mori, Alexandra Jilkine, and Leah Edelstein-Keshet. Asymptotic and bifurcation analysis of wave-pinning in a reaction-diffusion model for cell polarization. *SIAM journal on applied mathematics*, 71(4):1401–1427, 2011.
- 18 Catherine D Nobes and Alan Hall. Rho, rac, and cdc42 gtpases regulate the assembly of multimolecular focal complexes associated with actin stress fibers, lamellipodia, and filopodia. *Cell*, 81(1):53–62, 1995.
- 19 Mikiya Otsuji, Shuji Ishihara, Kozo Kaibuchi, Atsushi Mochizuki, Shinya Kuroda, et al. A mass conserved reaction–diffusion system captures properties of cell polarity. *PLoS computational biology*, 3(6):e108, 2007.
- 20 Marten Postma, Leonard Bosgraaf, Harriët M Looovers, and Peter JM Van Haastert. Chemotaxis: signalling modules join hands at front and tail. *EMBO reports*, 5(1):35–40, 2004.
- 21 Myrto Raftopoulou and Alan Hall. Cell migration: Rho gtpases lead the way. *Developmental biology*, 265(1):23–32, 2004.
- 22 Padmini Rangamani, Marc-Antoine Fardin, Yuguang Xiong, Azi Lipshtat, Olivier Rossier, Michael P Sheetz, and Ravi Iyengar. Signaling network triggers and membrane physical properties control the actin cytoskeleton-driven isotropic phase of cell spreading. *Biophysical journal*, 100(4):845–857, 2011.
- 23 Padmini Rangamani, Azi Lipshtat, Evren U Azeloglu, Rhodora Cristina Calizo, Mufeng Hu, Saba Ghassemi, James Hone, Suzanne Scarlata, Susana R Neves, and Ravi Iyengar. Decoding information in cell shape. *Cell*, 154(6):1356–1369, 2013.
- 24 Karin Rei, Catherine D Nobes, George Thomas, Alan Hall, and Doreen A Cantrell. Phosphatidylinositol 3-kinase signals activate a selective subset of rac/rho-dependent effector pathways. *Current Biology*, 6(11):1445–1455, 1996.
- 25 Jörg Schultz, Frank Milpetz, Peer Bork, and Chris P Ponting. Smart, a simple modular architecture research tool: identification of signaling domains. *Proceedings of the National Academy of Sciences*, 95(11):5857–5864, 1998.
- 26 Steven H Strogatz. *Nonlinear dynamics and chaos: with applications to physics, biology and chemistry*. Perseus publishing, 2001.
- 27 KK Subramanian and Atul Narang. A mechanistic model for eukaryotic gradient sensing: spontaneous and induced phosphoinositide polarization. *Journal of theoretical biology*, 231(1):49–67, 2004.
- 28 Philipp Khuc Trong, Ernesto M Nicola, Nathan W Goehring, K Vijay Kumar, and Stephan W Grill. Parameter-space topology of models for cell polarity. *New Journal of Physics*, 16(6):065009, 2014.
- 29 Alan Mathison Turing. The chemical basis of morphogenesis. *Philosophical Transactions of the Royal Society of London. Series B, Biological Sciences*, 237(641):37–72, 1952.
- 30 Georg R Walther, Athanasius FM Marée, Leah Edelstein-Keshet, and Verónica A Grieneisen. Deterministic versus stochastic cell polarisation through wave-pinning. *Bulletin of mathematical biology*, 74(11):2570–2599, 2012.
- 31 Wen Xiong and James E Ferrell. A positive-feedback-based bistable memory module that governs a cell fate decision. *Nature*, 426(6965):460–465, 2003.
- 32 Yuguang Xiong, Padmini Rangamani, Marc-Antoine Fardin, Azi Lipshtat, Benjamin Dubin-Thaler, Olivier Rossier, Michael P Sheetz, and Ravi Iyengar. Mechanisms controlling cell size and shape during isotropic cell spreading. *Biophysical journal*, 98(10):2136–2146, 2010.